

## Detectability of rotation-powered pulsars in future hard X-ray surveys \*

Wei Wang

National Astronomical Observatories, Chinese Academy of Sciences, Beijing 100012, China;  
[wangwei@bao.ac.cn](mailto:wangwei@bao.ac.cn)

Received 2009 May 5; accepted 2009 June 30

**Abstract** Recent INTEGRAL/IBIS hard X-ray surveys have detected about 10 young pulsars. We show hard X-ray properties of these 10 young pulsars, which have a luminosity of  $10^{33} - 10^{37}$  erg s<sup>-1</sup> and a photon index of 1.6–2.1 in the energy range of 20–100 keV. The correlation between X-ray luminosity and spin-down power of  $L_X \propto L_{sd}^{1.31}$  suggests that the hard X-ray emission in rotation-powered pulsars is dominated by the pulsar wind nebula (PWN) component. Assuming spectral properties are similar in 20–100 keV and 2–10 keV for both the pulsar and PWN components, the hard X-ray luminosity and flux of 39 known young X-ray pulsars and 8 millisecond pulsars are obtained, and a correlation of  $L_X \propto L_{sd}^{1.5}$  is derived. About 20 known young X-ray pulsars and 1 millisecond pulsars could be detected with future INTEGRAL and HXMT surveys. We also carry out Monte Carlo simulations of hard X-ray pulsars in the Galaxy and the Gould Belt, assuming values for the pulsar birth rate, initial position, proper motion velocity, period, and magnetic field distribution and evolution based on observational statistics and the  $L_X - L_{sd}$  relations:  $L_X \propto L_{sd}^{1.31}$  and  $L_X \propto L_{sd}^{1.5}$ . More than 40 young pulsars (mostly in the Galactic plane) could be detected after ten years of INTEGRAL surveys and the launch of HXMT. So, the young pulsars would be a significant part of the hard X-ray source population in the sky, and will contribute to unidentified hard X-ray sources in present and future hard X-ray surveys by INTEGRAL and HXMT.

**Key words:** pulsars: general — stars: neutron — X-rays: stars — radiation mechanisms: nonthermal

### 1 INTRODUCTION

High energy emission from rotation-powered pulsars directly reflects the acceleration processes of relativistic particles in the extreme astrophysical environment of pulsars. The detection of high energy radiation pulsars can be used to probe pulsar magnetospheric astrophysics, particle acceleration processes and the surrounding environment of pulsars, so studying the high energy properties of rotation-powered pulsars and searching for more high energy radiation pulsars are always the goals of pulsar research. In the soft X-ray band of 0.1–10 keV, more than 50 X-ray pulsars have been discovered with the launches of high resolution telescopes Chandra and XMM-Newton (see Becker & Aschenbach 2002;

---

\* Supported by the National Natural Science Foundation of China.

Kargaltsev & Pavlov 2008). Also, more than 30 gamma-ray pulsars have been detected with the all sky surveys of EGRET aboard the Compton observatory (Thompson 2001) and the new gamma-ray telescope FERMI/LAT (Abdo et al. 2008, 2009), while, in the intermediate energy bands (hard X-rays to soft gamma-rays: 20–1 MeV), a very small number of rotation-powered pulsars have been detected due to the sensitivity limits of telescopes (e.g., BeppoSAX, RXTE) and limited survey sky regions. Recently, a new soft gamma-ray telescope INTEGRAL was launched to perform the first all sky hard X-ray/soft gamma-ray survey (5 keV–8 MeV, Winkler et al. 2003). The four years of INTEGRAL observations have detected more than 400 hard X-ray sources in the energy range of 20–100 keV (Bird et al. 2007). Nine rotation-powered young pulsars are listed in the third soft gamma-ray catalog (Bird et al. 2007). Also, more than 100 hard X-ray sources are still unidentified; most of them are distributed in the Galactic plane (Bird et al. 2007), part of which would be attributed to unresolved or undetected pulsars.

High energy radiation of pulsars can originate from the pulsar surface/magnetosphere or from pulsar wind nebulae. Determining which component dominates the high energy radiation and resolving the two components are the key problems in recent pulsar studies. With high angular resolution (FWHM  $\sim 1''$ ), Chandra can directly resolve the pulsar wind nebula component from the pulsar component in imaging analysis of soft X-ray bands: 0.1–10 keV (Kargaltsev & Pavlov 2008 and the references therein). The derived X-ray luminosities of both pulsars and pulsar wind nebula (PWN) components correlate to the spin-down power of pulsars (Kargaltsev & Pavlov 2008), but these two components have different behaviors (Li et al. 2008):  $L_{X,2-10\text{ keV}} \propto L_{\text{sd}}^{0.92 \pm 0.04}$  for the pulsar component and  $L_{X,2-10\text{ keV}} \propto L_{\text{sd}}^{1.45 \pm 0.08}$  for the PWN component. In addition, for young energetic pulsars, the luminosity of the PWN component is generally much higher than that of the pulsar component from image-resolved studies, leading to the conclusion that the PWN component dominates X-ray radiation from 2–10 keV, which is also consistent with the results from the statistical studies of X-ray luminosity versus spin-down power (Cheng et al. 2004). Presently, studying hard X-ray properties (e.g. 10–300 keV) of pulsars is just beginning. With poor angular resolution (FWHM  $> 10'$  for INTEGRAL), hard X-ray imaging cannot resolve the pulsar emission from PWNe. Which component is dominant in the hard X-ray band? It is still unclear. INTEGRAL observations of some young pulsars generally suggest that the hard X-rays should be attributed to the PWN component (see Forot et al. 2006; Dean et al. 2008a,b; McBride et al. 2008; De Rosa et al. 2009). Since PWNe only contribute to non-pulsed emission, and high energy emission from the pulsar magnetosphere are mostly pulsed, then another possible way to resolve the pulsar component from the nebula component is by using a phase-resolved study. However, due to the limits of present sensitivity, only few pulsars (like the Crab) can be analyzed (see Mineo et al. 2006), and for most weaker hard X-ray pulsars, it is still impossible. With more ongoing INTEGRAL observations and improving sensitivities, phase-resolved studies of more hard X-ray pulsars would be a more promising way to probe the nature of these emissions.

INTEGRAL will continue with its observations, covering more sky regions and improving sensitivity. The new hard X-ray telescope, the Hard X-ray Modulation Telescope (HXMT), will be launched around 2011, and will perform all sky hard X-ray surveys in the energy range of 3–200 keV with higher sensitivity. More and deeper observations and new telescopes will push forward studies of hard X-ray pulsars. More rotation-powered pulsars will be detected and discovered in hard X-rays. With a good correlation between obtained luminosity versus spin-down power, we can predict hard X-ray luminosity/flux of pulsars in the Galaxy which may be unidentified, when we know the pulsar parameters, like spin period, magnetic field, distance, etc. Therefore, we apply a statistical approach using Monte Carlo simulations to study the unidentified hard X-ray pulsars in the Galaxy. We will simulate the galactic pulsar population and use the correlation of luminosity versus spin-down power to estimate the 20–100 keV hard X-ray flux of simulated pulsars. Unidentified hard X-ray pulsars could contribute to unidentified INTEGRAL sources and more hard X-ray pulsars could be detected in the future.

In Section 2, properties of 10 hard X-ray pulsars observed by IBIS are presented. In Section 3, hard X-ray properties of 39 young pulsars and 8 millisecond pulsars are predicted by extrapolating from their 2–10 keV properties to the 20–100 keV band. The correlation of hard X-ray luminosity versus spin-down power is constrained with these predicted pulsar samples. In Section 4, we describe the Monte

Carlo simulations to derive the distribution of young pulsars in the Galaxy and Gould Belt in the past 10 Myr, and predict hard X-ray luminosity/flux using the correlation of luminosity versus spin-down power. In Section 5, the distribution of the 20–100 keV hard X-ray flux can be used to predict the pulsar number possibly detected by future INTEGRAL and HXMT surveys. Finally, we present our summary and discussions in Section 6.

## 2 PROPERTIES OF OBSERVED ROTATION-POWERED HARD X-RAY PULSARS

We collected hard X-ray observational data of 10 young pulsars from the published literature. The observed parameters, detected fluxes and spectral properties of the 10 young pulsars detected by INTEGRAL/IBIS are presented in Table 1. The spin periods of the 10 pulsars are all below 0.4 s, the ages below  $\sim 50$  kyr, and the spin-down power higher than  $10^{36}$  erg s $^{-1}$ . These characteristics of the 10 pulsars suggest that energetic young pulsars should be the most probable hard X-ray sources. The hard X-ray luminosities (20–100 keV) of the 10 young pulsars vary from  $10^{33}$  –  $10^{37}$  erg s $^{-1}$ , and the photon index in this energy band is in the range 1.6–2.1 (except for the weak source PSR J1809–1917, see Dean et al. 2008a).

**Table 1** Characteristics of Spin Powered Pulsars and Their Hard X-ray Luminosities Observed by IBIS

PSR	$P$ (s)	Age (yr)	$d$ (kpc)	$L_{sd}$	$f$ (20–100 keV)	$L_X$ (20–100 keV)	Photon Index	Refs
B0531+21	0.033	1024	2	$4.5 \times 10^{38}$	$1.9 \pm 0.02 \times 10^{-8}$	$1.1 \pm 0.03 \times 10^{37}$	$2.10 \pm 0.01$	Mineo et al. (2006)
B0540–693	0.05	1670	49.4	$1.5 \times 10^{38}$	$3.2 \pm 0.9 \times 10^{-11}$	$9.3 \pm 3.1 \times 10^{36}$	$2.0 \pm 0.2$	Campana et al. (2008)
B0833–45	0.089	$1.13 \times 10^4$	0.29	$6.9 \times 10^{36}$	$1.5 \pm 0.3 \times 10^{-10}$	$2.1 \pm 0.8 \times 10^{33}$	$1.61 \pm 0.19$	Bird et al. (2007)
B1509–58	0.15	1550	5.81	$1.8 \times 10^{37}$	$1.7 \pm 0.1 \times 10^{-10}$	$6.8 \pm 0.6 \times 10^{35}$	$1.8 \pm 0.2$	Forot et al. (2006)
J1617–5055	0.069	8130	6.46	$1.6 \times 10^{37}$	$1.53 \pm 0.30 \times 10^{-11}$	$7.6 \pm 1.9 \times 10^{34}$	$2.1 \pm 0.3$	Bird et al. (2007)
J1809–1917	0.083	$5.13 \times 10^4$	3.71	$1.8 \times 10^{36}$	$2.5 \pm 2.1 \times 10^{-12}$	$3.9 \pm 3.3 \times 10^{33}$	–	Dean et al. (2008a)
J1811–1925	0.065	$2.23 \times 10^4$	5	$6.4 \times 10^{36}$	$1.5 \pm 0.4 \times 10^{-11}$	$4.5 \pm 1.6 \times 10^{34}$	$1.8 \pm 0.4$	Dean et al. (2008a)
J1833–1034	0.062	4850	4.3	$4.3 \times 10^{37}$	$5.6 \pm 0.4 \times 10^{-11}$	$1.3 \pm 0.2 \times 10^{35}$	$2.1 \pm 0.2$	De Rosa et al. (2009)
J1838–0655	0.07	$2.27 \times 10^4$	6.6	$5.5 \times 10^{36}$	$4.2 \pm 0.3 \times 10^{-11}$	$2.1 \pm 0.3 \times 10^{35}$	$1.8 \pm 0.3$	Gotthelf & Halpern (2008)
J1846–0258	0.326	728	5.1	$8.1 \times 10^{36}$	$3.55 \pm 0.20 \times 10^{-11}$	$1.1 \pm 0.2 \times 10^{35}$	$1.8 \pm 0.1$	McBride et al. (2008)

Notes: PSR is the pulsar name,  $P$  is the spin period,  $d$  is the distance of the pulsar from us in units of kpc.  $L_{sd}$  is the pulsar's spin-down power in units of erg s $^{-1}$ .  $f$  is the total hard X-ray flux observed by IBIS (20–100 keV) in units of erg cm $^{-2}$  s $^{-1}$ , and  $L_X$  is the observed total hard X-ray luminosity (erg s $^{-1}$ ) in the range 20–100 keV.

With the observed data from the present IBIS observations, we could study the possible correlation between the observed hard X-ray luminosity and the age/spin-down power of young pulsars. In order to evaluate the significance level of the correlation of two parameters, we also calculated the Spearman rank correlation coefficient ( $r$ ) and the probability ( $p$ ) of chance correlation from the Spearman rank test.

In Figure 1, we plot the hard X-ray luminosity versus the spin-down power of the 10 observed pulsars. We find that there could exist a correlation between  $L_X$  and  $L_{sd}$  which was supported by the Spearman test:  $r = 0.94463$ ,  $p < 0.0001$ . The solid line is the best fitting function  $L_X = 10^{-13.6 \pm 0.6} L_{sd}^{1.31 \pm 0.03}$ . For a comparison, we also plot other possible relations of  $L_X - L_{sd}$  in Figure 1. Becker & Trümper (1997) used the ROSAT data to find that the X-ray luminosity of pulsars in the band of 0.1–2 keV correlates with their spin-down power with a linear relation of  $L_X = 10^{-3} L_{sd}$  (see the dotted line in Fig. 1). Saito (1998) found a relation of  $L_X = 10^{-21} L_{sd}^{3/2}$  (see the dash-dotted line in Fig. 1) for the X-ray luminosity in the band of 2–10 keV based on ASCA data. The correlation of  $L_X = 10^{-21} L_{sd}^{3/2}$  seems to fit the data points well. However, the linear relation of  $L_X = 10^{-3} L_{sd}$  is far away from the observed data points. These more luminous hard X-ray pulsars (except for the Vela pulsar and PSR J1809–1917) have an efficiency ( $\eta = L_X/L_{sd}$ ) of around several percent, much higher than 0.001, which is found in the soft X-ray band (0.1–2 keV). The dashed line represents  $L_X = 0.01 L_{sd}$ . The data points of eight luminous hard X-ray pulsars look to be consistent with this relation.

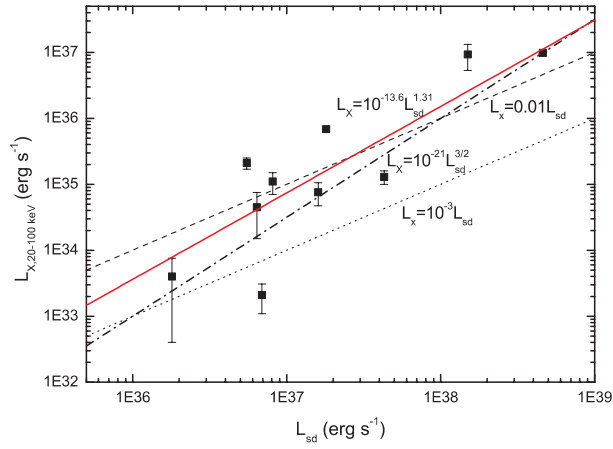


**Fig. 1** Observed hard X-ray luminosity (20–100 keV) from INTEGRAL/IBIS observations versus spin-down power of 10 young pulsars. The solid line is the best fitting function  $L_X = 10^{-13.6} L_{sd}^{1.31}$ . The dashed line is  $L_X = 0.01 L_{sd}$ , the dotted line represents  $L_X = 10^{-3} L_{sd}$ , and the dash-dotted line is  $L_X = 10^{-21} L_{sd}^{3/2}$ .

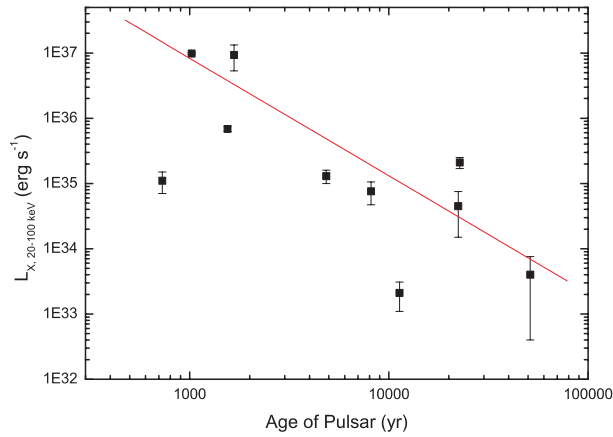


**Fig. 2** Observed hard X-ray luminosity (20–100 keV) from INTEGRAL/IBIS observations versus the age ( $\tau$ ) of 10 young pulsars. The solid line is the best fitting function  $L_X = 10^{42.2} \tau^{-1.80}$ .

The relation between the hard X-ray luminosity and the characteristic age ( $\tau = 2P/\dot{P}$ ) of pulsars is also plotted in Figure 2. Older pulsars have relatively lower X-ray luminosities ( $r = -0.7789$ ,  $p = 0.0068$ ). We found that a function of  $L_X = 10^{42.2 \pm 0.8} \tau^{-1.80 \pm 0.16}$  can fit this correlation.

## 2.1 Origin of Hard X-rays from Rotation-powered Pulsars

High energy emission from pulsars generally comes from two regions: inside the light cylinder ( $R_{LC} = c/\Omega = cP/2\pi$ ) and outside the light cylinder. Inside  $R_{LC}$ , high energy radiation can contribute to thermal emission from the pulsar surface and non-thermal emission from the pulsar magnetosphere. The thermal emission from the pulsar surface (e.g., the polar cap) contributes to soft X-rays (below  $\sim$

2 keV), and non-thermal emission (mostly pulsed) from the open field line region of the pulsar magnetosphere can contribute from X-rays to gamma-rays, covering the energy band from keV to GeV. Outside  $R_{LC}$ , a large number of relativistic particles escaping from pulsars interact with the surrounding medium and form PWNe. The magnetohydrodynamical shock in PWNe accelerates  $e^+e^-$  pairs to emit high energy photons from X-rays (through synchrotron radiation) to gamma-rays (inverse Compton scattering) covering the energy band from keV to TeV. This radiation component is non-thermal and non-pulsed.

These different high energy emission components could follow different  $L_{\text{rad}} - L_{\text{sd}}$  relations even for the same component in different energy bands. As we know, a correlation of the form  $L_X \propto L_{\text{sd}}^{1.39 \pm 0.25}$  was found in the Einstein data (0.7–8 keV) by Seward & Wang (1988). Subsequent studies using a larger sample of pulsars led to a relation of the form  $L_X \propto L_{\text{sd}}^{1.03 \pm 0.08}$  based on ROSAT data (0.1–2 keV, Becker & Trümper 1997) and  $L_X \propto L_{\text{sd}}^{1.5}$  based on ASCA data (2–10 keV, Saito 1998). A re-analysis of 39 pulsars based on data obtained from several X-ray satellites by Possenti et al. (2002) led to an intermediate relation  $L_X \propto L_{\text{sd}}^{1.34 \pm 0.03}$  (for 2–10 keV). However, these studies have not resolved the emission of the pulsar itself from the PWN component, and  $L_X$  was defined as the total X-ray luminosity. Wang & Zhao (2004) found the pulsed emission component of pulsars still follows a linear relation of  $L_X = 10^{-3} L_{\text{sd}}$  in the band of 0.1–2.4 keV, and Cheng et al. (2004) obtained the relations  $L_X \propto L_{\text{sd}}^{1.20 \pm 0.08}$  for the pulsed component and  $L_X \propto L_{\text{sd}}^{1.4 \pm 0.1}$  for the non-pulsed component in the band of 2–10 keV using ASCA data. Furthermore, using a simple PWN model, Cheng et al. (2004) also derived a relation of  $L_X \propto L_{\text{sd}}^{p/2}$ , where  $p \simeq 2.2 - 3$  is the energy index of accelerated electrons in the shock of PWNe, and then suggested that the X-ray emission from pulsars in the band of 2–10 keV should be dominated by the PWN component. Chandra and XMM-Newton observations can now resolve the pulsars from the surrounding PWNe with high spatial resolution. Recent analysis using Chandra and XMM-Newton results reported correlations of  $L_X \propto L_{\text{sd}}^{0.92 \pm 0.04}$  for the 2–10 keV X-ray luminosity versus spin-down power of the pulsars and  $L_X \propto L_{\text{sd}}^{1.45 \pm 0.08}$  for the PWN component (Li et al. 2008). We also note that the pulsed GeV emission from gamma-ray pulsars versus the spin-down power follows a relation  $L_\gamma \propto L_{\text{sd}}^{0.5}$  (Thompson 2001).

The deduced existence of correlations between X-ray/gamma-ray luminosities and spin-down power suggests that the observed luminosities are produced by a process which taps the rotational energy of the neutron star. Though a detailed description of the mechanism inducing these correlations remains elusive, present statistical studies can help us to probe the nature of high energy emission and determine which component dominates radiation in different energy bands.

Due to the limits of observational ability in present hard X-ray telescopes, e.g. poor angular resolution, and low sensitivity, we cannot resolve the pulsar component from the nebulae component in the hard X-ray band. However, hard X-rays (20–100 keV) from young pulsars follow a relation of  $L_X \propto L_{\text{sd}}^{1.31}$ . This relation is similar to the correlation between X-ray luminosity of PWNe and pulsar spin-down power in 2–10 keV (Cheng et al. 2004; Li et al. 2008). So, our statistical studies of hard X-ray pulsars suggest that 20–100 keV radiation of pulsars is mainly attributed to the PWN component. Here, we conclude that soft X-ray emission from 0.1–2 keV is dominated by the pulsar component, hard X-ray to soft gamma-ray emission (2–100 keV) is dominated by the PWN component, and GeV gamma-ray emission is dominated by the pulsar component.

### 3 HARD X-RAY LUMINOSITY VERSUS SPIN-DOWN POWER OF PULSARS

In Section 2, the relation between 20–100 keV hard X-ray luminosities of 10 pulsars and spin down power is studied. From this correlation, we find that the hard X-rays from rotation-powered pulsars are dominated by the PWN component, which is similar to the case with a 2–10 keV X-ray origin. In the energy band of 2–10 keV, the 10 hard X-ray pulsars have also been observed by Chandra and XMM-Newton. With high angular resolution and sensitivity, Chandra and XMM-Newton can resolve the pulsar emission from the PWN component. So, we collected the X-ray luminosities and spectral indices of the 10 pulsars and their PWNe in the band of 2–10 keV observed by Chandra and XMM-Newton from the published literature (see Table 2).

**Table 2** Properties of 39 Young X-ray Pulsars and Their Pulsar Wind Nebulae and Predicted Hard X-ray Luminosities and Fluxes

PSR	$L_{\text{sd}}$	$L_{\text{PSR}}$	$\Gamma_{\text{PSR}}$	$L_{\text{PWN}}$	$\Gamma_{\text{PWN}}$	$L_{\text{HX,pred}}$	$F_{\text{pred}}$	Refs
J0205+6449	$2.7 \times 10^{37}$	$9.1^{+1.2} \times 10^{32}$	$1.8 \pm 0.2$	$6.8^{+1.1} \times 10^{33}$	$2.07 \pm 0.2$	$7.0^{+6.1} \times 10^{33}$	$5.7^{+4.9} \times 10^{-12}$	SL04
B0355+54	$4.5 \times 10^{34}$	$3.9^{+0.3} \times 10^{30}$	$1.5 \pm 0.7$	$1.7^{+0.2} \times 10^{31}$	$1.3^{+0.4}$	$7.7^{+5.9} \times 10^{32}$	$5.9^{+4.3} \times 10^{-12}$	MC06
B0531+21	$4.6 \times 10^{38}$	$1.1^{+0.1} \times 10^{36}$	$2.0 \pm 0.2$	$1.0^{+0.1} \times 10^{37}$	$2.11^{+0.01}$	$1.0^{+0.4} \times 10^{37}$	$2.1^{+0.9} \times 10^{-8}$	MO04
J0537-6910	$4.9 \times 10^{38}$	$5.1^{+0.6} \times 10^{35}$	$1.8 \pm 0.2$	$1.0^{+0.1} \times 10^{36}$	$2.2 \pm 0.2$	$1.1^{+0.7} \times 10^{36}$	$3.7^{+3.0} \times 10^{-12}$	CH06
J0538+2817	$4.9 \times 10^{34}$	$5.7^{+1.9} \times 10^{30}$	$1.5 \pm 0.7$	$1.0^{+0.2} \times 10^{31}$	$3.3 \pm 0.5$	$2.0^{+1.8} \times 10^{31}$	$7.8^{+6.5} \times 10^{-14}$	RO03
B0540-69	$1.5 \times 10^{38}$	$1.3^{+0.4} \times 10^{36}$	$2.05^{+0.08}$	$7.3^{+1.2} \times 10^{36}$	$1.9^{+0.2}$	$8.9^{+3.2} \times 10^{36}$	$1.5^{+0.8} \times 10^{-11}$	KA03
J0631+1036	$1.7 \times 10^{35}$	$2.0^{+0.3} \times 10^{32}$	$2.3 \pm 0.5$	$2.2^{+0.3} \times 10^{32}$	$3.5 \pm 0.9$	$2.0^{+1.6} \times 10^{32}$	$3.9^{+2.9} \times 10^{-14}$	TO01
J0633+1746	$3.2 \times 10^{34}$	$2.1^{+0.5} \times 10^{30}$	$1.56^{+0.24}$	$1.1^{+0.3} \times 10^{29}$	$1.0^{+0.2}$	$4.3^{+3.8} \times 10^{30}$	$5.7^{+5.0} \times 10^{-13}$	CA03
B0656+14	$3.8 \times 10^{34}$	$9.5^{+3.2} \times 10^{29}$	$2.1 \pm 0.3$	-	-	$9^{+7} \times 10^{29}$	$1.3^{+1.0} \times 10^{-14}$	DE05
J0729-1448	$2.8 \times 10^{35}$	$2.5^{+0.5} \times 10^{31}$	$1.8 \pm 0.3$	$2.1^{+0.6} \times 10^{31}$	$1.8 \pm 0.4$	$1.1^{+1.0} \times 10^{32}$	$5.7^{+5.2} \times 10^{-14}$	PE02
B0833-45	$6.9 \times 10^{36}$	$3.3^{+0.5} \times 10^{31}$	$2.0 \pm 0.3$	$6.1^{+0.7} \times 10^{32}$	$1.4 \pm 0.2$	$2.2^{+1.3} \times 10^{33}$	$2.1^{+1.3} \times 10^{-10}$	HE01
J1016-5857	$2.6 \times 10^{36}$	$6.1^{+1.1} \times 10^{31}$	$1.5 \pm 0.4$	$2.5^{+0.5} \times 10^{32}$	$1.3^{+0.4}$	$3.1^{+2.6} \times 10^{33}$	$2.8^{+2.2} \times 10^{-12}$	CG04
B1046-58	$2 \times 10^{36}$	$2.9^{+0.6} \times 10^{31}$	$1.5 \pm 0.3$	$6.0^{+1.2} \times 10^{31}$	$1.0^{+0.2}$	$7^{+5} \times 10^{32}$	$6.5^{+5.1} \times 10^{-13}$	GN06
B1055-52	$3.0 \times 10^{34}$	$4.5^{+2.0} \times 10^{30}$	$1.7 \pm 0.3$	-	-	$9.0^{+7.2} \times 10^{30}$	$1.5^{+1.2} \times 10^{-13}$	KR03
J1119-6127	$2.3 \times 10^{36}$	$9.6^{+0.6} \times 10^{32}$	$1.5 \pm 0.3$	$1.0^{+0.2} \pm 10^{33}$	$1.5 \pm 0.2$	$6.0^{+4.5} \times 10^{33}$	$7.1^{+5.3} \times 10^{-13}$	GN03
J1124-5916	$1.2 \times 10^{37}$	$4.1^{+1.1} \times 10^{33}$	$1.6 \pm 0.1$	$5.9^{+0.9} \times 10^{34}$	$1.8 \pm 0.2$	$1.2^{+0.5} \times 10^{35}$	$2.7^{+1.2} \times 10^{-11}$	HU01
J1301-6305	$1.65 \times 10^{36}$	$7.9^{+0.7} \times 10^{32}$	$2.0 \pm 0.2$	$1.9^{+0.4} \times 10^{32}$	$2.0 \pm 0.2$	$1.0^{+0.9} \times 10^{33}$	$1.7^{+1.2} \times 10^{-13}$	KP07a
J1357-6429	$3 \times 10^{36}$	$2.2^{+0.6} \times 10^{32}$	$1.3 \pm 0.2$	$3.1^{+1.5} \times 10^{31}$	$1.8 \pm 0.2$	$8^{+6} \times 10^{32}$	$1.0^{+0.8} \times 10^{-12}$	ZA07
J1420-6048	$1 \times 10^{37}$	$7.5^{+2.5} \times 10^{32}$	$1.0 \pm 0.5$	$1.4^{+0.4} \times 10^{33}$	$0.5^{+1.2}$	$5.0^{+4.8} \times 10^{34}$	$1.3^{+1.2} \times 10^{-11}$	NG05
J1509-58	$1.8 \times 10^{37}$	$1.0^{+0.1} \times 10^{35}$	$1.2 \pm 0.1$	$4.1^{+0.5} \times 10^{34}$	$1.65^{+0.05}$	$7.9^{+2.0} \times 10^{35}$	$2.6^{+0.7} \times 10^{-10}$	GA02
J1617-5055	$1.6 \times 10^{37}$	$4.5^{+0.8} \times 10^{33}$	$1.19^{+0.11}$	$1.2^{+0.1} \times 10^{34}$	$1.15^{+0.2}$	$1.1^{+0.7} \times 10^{35}$	$2.1^{+1.1} \times 10^{-11}$	GA02
B1702-4128	$3.4 \times 10^{35}$	$4.3^{+1.2} \times 10^{31}$	$2.0 \pm 0.3$	$3.5^{+0.9} \times 10^{31}$	$2.0 \pm 0.3$	$7.8^{+5.7} \times 10^{31}$	$2.0^{+1.8} \times 10^{-14}$	PE02
B1706-44	$3.4 \times 10^{36}$	$9.8^{+0.9} \times 10^{31}$	$2.0 \pm 0.3$	$3.5^{+0.8} \times 10^{32}$	$1.3 \pm 0.2$	$1.8^{+1.2} \times 10^{33}$	$3.8^{+2.2} \times 10^{-12}$	RN05
J1718-3825	$1.26 \times 10^{36}$	$3.1^{+0.9} \times 10^{32}$	$1.4 \pm 0.2$	$3.9^{+0.9} \times 10^{32}$	$1.9 \pm 0.2$	$1.6^{+1.2} \times 10^{33}$	$8.3^{+6.2} \times 10^{-13}$	HI07
J1740+10	$2.3 \times 10^{35}$	$3.1^{+0.6} \times 10^{30}$	$1.3 \pm 0.3$	$1.0^{+0.2} \times 10^{31}$	$1.5 \pm 0.3$	$2.0^{+1.7} \times 10^{32}$	$8.5^{+7.6} \times 10^{-13}$	PE02
J1747-2958	$2.5 \times 10^{36}$	$9.9^{+2.9} \times 10^{33}$	$1.4 \pm 0.1$	$1.4^{+0.3} \times 10^{34}$	$1.9 \pm 0.1$	$5.5^{+4.5} \times 10^{34}$	$1.8^{+1.6} \times 10^{-11}$	GA04
B1757-24	$2.6 \times 10^{36}$	$1.9^{+0.7} \times 10^{33}$	$1.9 \pm 0.3$	$1.8^{+0.6} \times 10^{33}$	$2.5 \pm 0.3$	$2.4^{+1.9} \times 10^{33}$	$8.3^{+6.6} \times 10^{-13}$	KI01
B1800-21	$2.2 \times 10^{36}$	$3.6^{+0.6} \times 10^{31}$	$1.4 \pm 0.6$	$1.7^{+0.4} \times 10^{32}$	$1.6 \pm 0.3$	$5.6^{+5.0} \times 10^{32}$	$2.9^{+2.6} \times 10^{-13}$	KP07b
J1809-1917	$1.8 \times 10^{36}$	$4.0^{+0.6} \times 10^{31}$	$1.2 \pm 0.6$	$3.8^{+0.3} \times 10^{32}$	$1.4 \pm 0.1$	$1.6^{+1.2} \times 10^{33}$	$1.0^{+0.8} \times 10^{-12}$	KP07a
J1811-1925	$6.4 \times 10^{36}$	$7.5^{+0.7} \times 10^{33}$	$1.4 \pm 0.1$	$1.0^{+0.1} \times 10^{34}$	$1.5 \pm 0.2$	$9.5^{+7.5} \times 10^{34}$	$3.2^{+2.7} \times 10^{-11}$	RB03
J1823-13	$2.8 \times 10^{36}$	$9.7^{+1.1} \times 10^{31}$	$1.9 \pm 0.7$	$3.2^{+0.7} \times 10^{32}$	$1.3 \pm 0.3$	$1.45^{+1.30} \times 10^{33}$	$7.5^{+7.0} \times 10^{-13}$	GA03
J1833-1034	$4.3 \times 10^{37}$	$2.2^{+0.3} \times 10^{35}$	$1.9 \pm 0.3$	$1.4^{+0.2} \times 10^{34}$	$1.5 \pm 0.1$	$3.2^{+1.7} \times 10^{35}$	$1.4^{+0.7} \times 10^{-10}$	SH01
J1838-0655	$5.5 \times 10^{36}$	$4.6^{+0.8} \times 10^{34}$	$0.5 \pm 0.3$	$5.2^{+0.9} \times 10^{33}$	$1.6 \pm 0.4$	$1.1^{+0.9} \times 10^{36}$	$2.1^{+1.8} \times 10^{-10}$	GH08
J1846-0258	$8.1 \times 10^{36}$	$3.3^{+0.4} \times 10^{33}$	$1.9 \pm 0.1$	$9.3^{+0.6} \times 10^{34}$	$1.89^{+0.05}$	$1.2^{+0.9} \times 10^{35}$	$3.8^{+3.2} \times 10^{-11}$	HF03
B1853+01	$4.3 \times 10^{35}$	$6.2^{+0.9} \times 10^{31}$	$1.3 \pm 0.5$	$2.1^{+0.6} \times 10^{32}$	$2.2 \pm 0.2$	$4.4^{+3.8} \times 10^{32}$	$4.0^{+3.2} \times 10^{-13}$	PE02
J1930+1852	$1.2 \times 10^{37}$	$5.4^{+0.7} \times 10^{33}$	$1.2 \pm 0.2$	$1.6^{+0.3} \times 10^{34}$	$1.9 \pm 0.1$	$5.4^{+4.5} \times 10^{34}$	$1.8^{+1.6} \times 10^{-11}$	LU02
B1951+32	$3.7 \times 10^{36}$	$3.9^{+0.6} \times 10^{32}$	$1.70^{+0.03}$	$2.2^{+0.9} \times 10^{33}$	$1.7 \pm 0.3$	$5.7^{+4.6} \times 10^{33}$	$7.6^{+6.2} \times 10^{-12}$	LI05
J2021+3651	$3.4 \times 10^{36}$	$2.3^{+0.4} \times 10^{32}$	$1.0 \pm 0.4$	$2.4^{+0.4} \times 10^{33}$	$1.7 \pm 0.3$	$5.6^{+3.7} \times 10^{33}$	$2.9^{+2.2} \times 10^{-12}$	HS04
J2229+6114	$2.2 \times 10^{37}$	$5.6^{+1.1} \times 10^{32}$	$1.5 \pm 0.1$	$8.6^{+0.9} \times 10^{32}$	$1.3 \pm 0.1$	$6.9^{+5.4} \times 10^{33}$	$5.4^{+4.6} \times 10^{-12}$	HL01

Notes: PSR is the pulsar name,  $L_{\text{sd}}$  is the pulsar's spin-down power in units of  $\text{erg s}^{-1}$ .  $L_{\text{HX,pred}}$  is the predicted total hard X-ray luminosity in the range of 20–100 keV, and  $F_{\text{pred}}$  is the predicted X-ray flux in the range of 20–100 keV.

Assuming that X-ray emissions in 2–10 keV can be extended to the energy band 20–100 keV without significant spectral break-off for both pulsar and PWN components:

$$F_{\text{psr}} \propto E^{-\Gamma_1}; \quad F_{\text{PWN}} \propto E^{-\Gamma_2}, \quad (1)$$

where  $\Gamma_1$  and  $\Gamma_2$  are the photon index of the pulsar and PWN respectively. Then, we can estimate the luminosities of pulsars and PWNe in the 20–100 keV:  $L_{\text{psr},20-100 \text{ keV}}$  and  $L_{\text{PWN},20-100 \text{ keV}}$ . The total hard X-ray luminosity of pulsars in 20–100 keV is

$$L_{20-100 \text{ keV}} = L_{\text{psr},20-100 \text{ keV}} + L_{\text{PWN},20-100 \text{ keV}}. \quad (2)$$

So, we can predict the hard X-ray luminosity of the 10 pulsars (Table 2, the uncertainties of extrapolated X-ray luminosity come from uncertainties of both soft X-ray luminosity and photon indices),

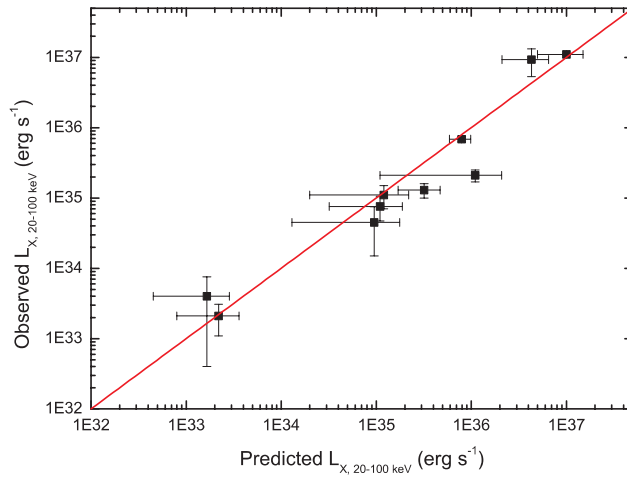


**Fig. 3** Observed hard X-ray luminosity (20–100 keV) from INTEGRAL/IBIS observations versus the predicted hard X-ray luminosity of 10 young pulsars. The predicted hard X-ray luminosity (20–100 keV) extracted from the X-ray properties in 2–10 keV is very consistent with the observed luminosity by IBIS.

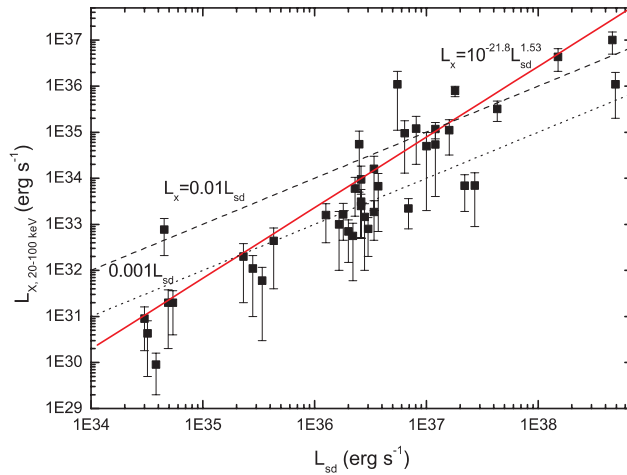


**Fig. 4** Predicted hard X-ray luminosity (20–100 keV) extracted from the X-ray properties in 2–10 keV versus spin-down power of 39 young pulsars. The solid line is the best fitting function  $L_X = 10^{-21.8} L_{sd}^{1.53}$ . The dashed line is  $L_X = 0.01 L_{sd}$ , the dotted line represents  $L_X = 10^{-3} L_{sd}$ .

and compare the predicted luminosity with the observed luminosity observed by INTEGRAL/IBIS (see Fig. 3). The predicted luminosity in 20–100 keV is very consistent with the observed one within error bars, confirming the above assumption and the conclusion in Section 2.1.

The present hard X-ray pulsar sample is still small. However, in softer X-ray bands of 0.1–10 keV, more than 50 X-ray pulsars (including X-ray millisecond pulsars) have been discovered with ROSAT, ASCA, Chandra and XMM-Newton observations. The comparison in Figure 3 implies that we can predict the hard X-ray luminosities of these X-ray pulsars by extending the observed 2–10 keV emission of pulsars to the band of 20–100 keV.

In Table 2, 39 young X-ray pulsars with spin-down power  $> 10^{34}$  erg s $^{-1}$  and X-ray luminosities and photon indices from the Chandra and XMM-Newton observations are collected from the published literature. In most of them, PWNe around pulsars have been detected. In this case, the luminosities and photon indices for both pulsars and PWNe (see Table 2) are used to predict the hard X-ray luminosity. Two of these young pulsars (PSR 0656+14, PSR 1055–52) do not yet show any evidence for PWN components with present X-ray observations. So, the luminosity and photon index of only the pulsar component are used in the predictions. Finally, we give the hard X-ray luminosities of 39 young pulsars in Table 2 (including 10 pulsars detected by INTEGRAL/IBIS).

With a large pulsar sample, we re-analyzed the relation between hard X-ray luminosity versus spin-down power for young pulsars, which is plotted in Figure 4. The best fitting function for these predicted data points is  $L_X = 10^{-21.8 \pm 0.4} L_{sd}^{1.53 \pm 0.02}$  ( $r = 0.99511$ ,  $p < 0.0001$ ). This correlation is very consistent with the correlation from ASCA  $L_X \propto L_{sd}^{1.5}$  (Saito 1998) and the relation between X-ray luminosity of PWNe and spin-down power in 2–10 keV (Li et al. 2008).

Millisecond pulsars (MSPs) in soft X-ray bands (0.1–10 keV) have been studied with different telescopes. Soft X-rays from MSPs are generally attributed to thermal emission from the heated polar caps of pulsars. Non-thermal hard spectra from 2–10 keV are also reported in some MSPs, like PSR J0218+4232 and PSR B1937+21 (see Table 3). X-ray PWNe around MSPs are also discovered by high resolution observations of Chandra (e.g., PSR B1957+20, Stappers et al. 2003). PSR J0218+4232 was detected in hard X-rays up to  $\sim 20 - 30$  keV by RXTE (Kuiper et al. 2004), and this MSP is also a gamma-ray pulsar candidate observed by EGRET (Kuiper et al. 2000). So, MSPs should be good candidates for hard X-ray sources, though INTEGRAL/IBIS have not reported the detection of MSPs with the present data (Bird et al. 2007).

**Table 3** Characteristics of 8 Millisecond X-ray Pulsars in the Galactic Disk and Predicted Hard X-ray Luminosities and Fluxes

PSR	$P$ (ms)	$d$ (kpc)	$L_{sd}$	$L_X$ (2–10 keV)	$\Gamma$	$L_{HX,pred}$	$F_{HX,pred}$	Refs
J0030+0451	4.87	0.23	$3.4 \times 10^{33}$	$1.8^{+0.3} \times 10^{29}$	$3^{+0.4}$	$1.0^{+0.8} \times 10^{29}$	$1.5^{+1.1} \times 10^{-14}$	BA02
J0218+4232	2.3	2.7	$2.5 \times 10^{35}$	$\frac{4.7^{+1.1} \times 10^{32a}}{3^{+0.9} \times 10^{31b}}$	$\frac{0.61^{+0.32a}}{1.17^{+0.37b}}$	$1.1^{+0.8} \times 10^{34}$	$1.2^{+0.9} \times 10^{-11}$	WE04a
J0437–47	5.8	0.139	$4.2 \times 10^{33}$	$2.0^{+0.3} \times 10^{29}$	$2.2^{+0.3}$	$1.3^{+0.9} \times 10^{29}$	$5.6^{+3.6} \times 10^{-14}$	ZA02
J0751+1807	3.48	1.1	$6 \times 10^{33}$	$3.9^{+0.8} \times 10^{30}$	$1.59^{+0.2}$	$1.0^{+0.6} \times 10^{31}$	$6.9^{+4.1} \times 10^{-14}$	WE04b
J1012+5307	5.3	0.77	$4 \times 10^{33}$	$4.0^{+0.7} \times 10^{30}$	$1.78^{+0.36}$	$6.3^{+5.0} \times 10^{30}$	$8.8^{+7.0} \times 10^{-14}$	WE04b
B1937+21	1.56	3.6	$1.1 \times 10^{36}$	$\frac{4.6^{+0.7} \times 10^{32a}}{1.8^{+0.4} \times 10^{32b}}$	$\frac{1.21^{+0.15a}}{3.3^{+0.5b}}$	$2.8^{+2.1} \times 10^{33}$	$1.8^{+1.2} \times 10^{-12}$	NI04
B1957+20	1.6	2.5	$1 \times 10^{35}$	$3.0^{+0.3} \times 10^{31}$	$1.9^{+0.5}$	$3.8^{+2.4} \times 10^{31}$	$5.1^{+3.2} \times 10^{-14}$	ST03
J2124–3358	4.93	0.25	$4.3 \times 10^{33}$	$1.9^{+0.2} \times 10^{29}$	$2.8^{+0.6}$	$1.2^{+0.95} \times 10^{29}$	$1.6^{+1.2} \times 10^{-14}$	SA01

Notes: PSR is the pulsar name,  $P$  is the spin period,  $d$  is the distance of the pulsar from us in units of kpc.  $L_X$  is the observed X-ray luminosity in the range of 2–10 keV,  $\Gamma$  is the photon index.  $L_{HX,pred}$  is the predicted total hard X-ray luminosity in the range of 20–100 keV,  $F_{HX,pred}$  is the predicted hard X-ray flux in the range of 20–100 keV.

<sup>a</sup> the pulsed component.

<sup>b</sup> the non-pulsed component.

X-ray properties in 2–10 keV of eight MSPs in the Galactic disk (X-rays are powered by rotational energy, not including MSPs in globular clusters and those in low mass X-ray binary systems) are collected in Table 3. Pulsed and non-pulsed X-ray emissions have been resolved in two MSPs, PSR J0218+4232 and PSR B1937+21, then X-ray luminosity and photon index for the two components are both presented. For other MSPs, only total X-ray luminosity and average photon index are used. Similar to the young pulsar case, we extended the 2–10 keV emissions of MSPs to the 20–100 keV band with the same assumption, and predicted the 20–100 keV luminosity of 8 MSPs (Table 3).

The predicted hard X-ray luminosity (20–100 keV) versus spin-down power of 39 young pulsars plus 8 MSPs is plotted in Figure 5. The data points can be fitted with a function of  $L_X = 10^{-20.8 \pm 0.4} L_{sd}^{1.49 \pm 0.02}$  ( $r = 0.96717$ ,  $p < 0.0001$ ). This correlation is also consistent with the  $L_X \propto L_{sd}^{1.5}$  relation.

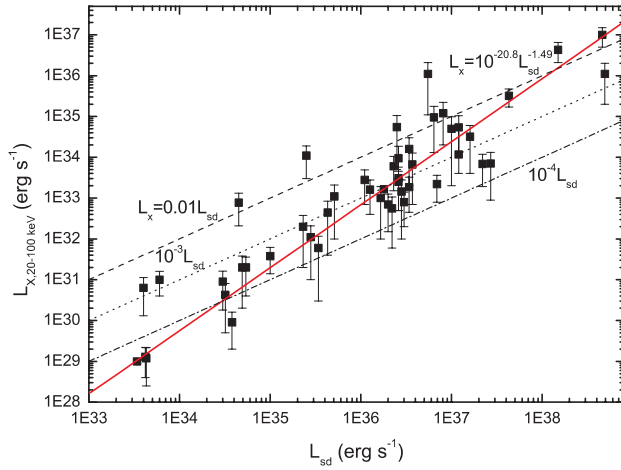


**Fig. 5** Predicted hard X-ray luminosity (20–100 keV) extracted from the X-ray properties in 2–10 keV versus spin-down power of 47 pulsars (including 8 MSPs in the Galactic disk). The solid line is the best fitting function  $L_X = 10^{-20.8} L_{sd}^{1.49}$ . The dashed line is  $L_X = 0.01 L_{sd}$ , the dotted line represents  $L_X = 10^{-3} L_{sd}$ , and the dash-dotted line is  $L_X = 10^{-4} L_{sd}$ .

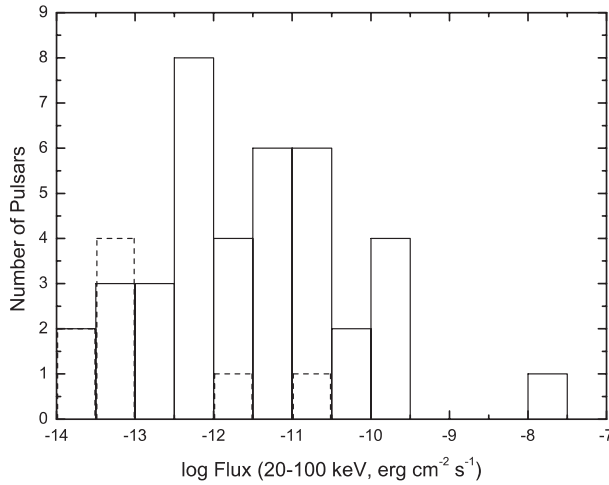


**Fig. 6** Distributions of the predicted hard X-ray flux (20–100 keV) for 39 young pulsars (*solid*, from Table 2) and 8 millisecond pulsars (*dashed*, from Table 3).

Knowing the hard X-ray luminosities of 39 young X-ray pulsars and 8 MSPs in the Galactic disk, and assuming the hard X-ray radiation is isotropic, we can derive predicted hard X-ray fluxes in the energy band of 20–100 keV of these known X-ray pulsars:  $F_X = L_X/4\pi d^2$  (see Tables 2 and 3). In Figure 6, we present 20–100 keV hard X-ray flux distributions of both 39 young pulsars and 8 MSPs. Currently, INTEGRAL/IBIS has detected only 10 young pulsars due to the limits of the hard X-ray survey depth which is estimated to be different for different sky regions (Bird et al. 2007):  $\sim 0.2$  mCrab in the inner Galactic plane ( $|l| < 30^\circ$ ,  $|b| < 5^\circ$ ), 0.3 mCrab for the other region of the Galactic plane, and 0.5 mCrab for the higher latitude region; 1 mCrab is about  $1.95 \times 10^{-11} \text{ erg cm}^{-2} \text{ s}^{-1}$  in

the band of 20–100 keV. Therefore, this is the reason that IBIS only detected PSR B540–69 in the Large Magellanic Cloud (LMC), while the other young energetic pulsar PSR J0537–6910 ( $F_{X,\text{pred}} \sim 3.7 \times 10^{-12} \text{ erg cm}^{-2} \text{ s}^{-1}$ , below the IBIS sensitivity) in LMC cannot be detected at present. The MSP (PSR J0218+4232) is predicted to have a hard X-ray flux  $> 10^{-11} \text{ erg cm}^{-2} \text{ s}^{-1}$ , and should be a potential hard X-ray source which could be searched for by INTEGRAL/IBIS in the next observations. If the future INTEGRAL/IBIS survey depth reaches  $\sim 0.15 \text{ mCrab}$  for all of the sky, 20 of 39 young X-ray pulsars and PSR J0218+4232 could be detected by IBIS.

#### 4 SIMULATIONS OF HARD X-RAY PULSARS IN THE GALAXY

In the above section, we have estimated the hard X-ray flux (20–100 keV) of known X-ray pulsars, and predicted potential hard X-ray source candidates by future INTEGRAL/IBIS observations. How many young pulsars in the Galaxy could be detected by future hard X-ray surveys? From the sample of known X-ray pulsars, there may be less than 20 young pulsars which are hard X-ray sources. With radio and softer X-ray ( $< 10 \text{ keV}$ ) searches, we still cannot identify all pulsars, e.g., the hard X-ray pulsar PSR J1838–0655 was identified as a young energetic pulsar with hard X-ray timing telescope RXTE (Gotthelf & Halpern 2008). Soft X-ray surveys (like ROSAT, 0.1–2.4 keV) are strongly affected by absorption along the Galactic plane, so pulsar search work is limited by this strong absorption. Also, high angular resolution and high sensitivity X-ray telescopes (like Chandra and XMM-Newton, 0.1–10 keV) only cover very small sky regions, so they are mainly used as follow-up high-precision studies. Hard X-rays to soft gamma-rays are nearly transparent with respect to the interstellar medium in the Galaxy, so all sky hard X-ray surveys are expected to discover more young pulsars, like the present INTEGRAL/IBIS survey (20–100 keV), the future Chinese HXMT<sup>1</sup> survey (20–300 keV) and the future eROSITA<sup>2</sup> (proposed by German scientists and scheduled to be launched around 2011) survey (2–20/30 keV). To answer the question we proposed initially, we carry out a Monte Carlo simulation of young pulsars in the Galaxy. Considering that some pulsars are located in nearby systems to the Sun, we also simulate the young pulsars in the Gould Belt region.

In this section, we briefly describe the Monte Carlo method which is used to simulate the properties of the luminosity, spatial evolution, and distributions of hard X-ray pulsars in the Galaxy. This Monte Carlo method has also been applied to simulate gamma-ray pulsars in the Galaxy (see Wang et al. 2005 and references therein).

##### 4.1 Monte Carlo Simulation of Hard X-ray Pulsars in the Galaxy

The basic assumptions and steps of our Monte Carlo simulation are given as follows:

1. The birth rate of pulsars in the Galaxy is not quite clear; it is about one pulsar every 50–200 yr. Here, we use a pulsar birth rate in the Galaxy of one pulsar per century. Basically, the birth rates will only affect the final number of hard X-ray pulsars, not their distributions.
2. The age of the Gould Belt is  $\sim 30 \text{ Myr}$ . The Sun is inside the Gould Belt and is located about 200 pc towards  $l = 130^\circ$  (Guilout et al. 1998). The Gould Belt has an ellipsoidal shaped ring with semi-major and minor axes equal to 500 pc and 340 pc, respectively. The birth rate of pulsars in the Gould Belt is also not certain, but a rate of  $20 \text{ Myr}^{-1}$  is generally used (Grenier 2000).
3. The initial position for each pulsar in the Galaxy is distributed according to the mass distribution of the Galaxy. We use the mass distribution suggested by Paczynski (1990) and Sturmer & Dermer (1996), but the initial position of each pulsar is assumed to be uniform inside the Gould Belt.
4. The initial magnetic field  $\log B$  is assumed to be Gaussian, with a mean value of 12.5 and a dispersion of 0.3. Since the pulsars in our simulation sample are all younger than 10 Myr, and the magnetic field does not decay in 10 Myr (Bhattacharya et al. 1992), we have ignored the field decay for these pulsars.

---

<sup>1</sup> <http://www.hmxt.cn/english/>

<sup>2</sup> <http://www.mpe.mpg.de/erosita/>

5. The initial period is chosen to be  $P_0 = 10$  ms, and the period at time  $t$  is given by  $P(t) = (P_0 + 1.95 \times 10^{-39} B^2 t)^{1/2}$ .
6. The initial velocity of each pulsar is the vector sum of the circular rotation velocity at the birth location and the random velocity from the supernova explosion (Paczynski 1990). The circular velocity is determined by the Galactic gravitational potential and the Maxwellian three-dimensional root-mean-square (rms) velocity which is assumed to be  $\sqrt{3} \times 100$  km s $^{-1}$  (Lorimer et al. 1997). Furthermore, the pulsar position at time  $t$  is determined following its motion in the Galactic gravitational potential. Using the equations given by Paczynski (1990) for the given initial velocity, orbital integrations are performed using the fourth-order Runge Kutta method with variable time steps on the variables  $R$ ,  $V_R$ ,  $z$ , and  $V_z$ . The sky positions and distances to the simulated pulsars can then be calculated.
7. The hard X-ray background may be non-uniform over the sky, and the exposure time for the different parts of the sky would also be quite different, therefore the hard X-ray threshold varies over the sky as well. In general, the threshold will be higher in the galactic plane and lower at higher latitudes. Also, it is accepted that a detectable source should at least have a signal of  $4.8\sigma$  above the background in the INTEGRAL all sky survey observations (Bird et al. 2007), which is roughly equivalent to the likelihood criterion  $\sqrt{TS} \geq 5$ . For the 4 years of INTEGRAL/IBIS observations, the sky survey depth is estimated to be up to  $\sim 0.2$  mCrab in the inner Galactic plane, 0.3 mCrab for the other region of the Galactic plane, and  $\sim 0.5$  mCrab for the higher latitude region, respectively (Bird et al. 2007). INTEGRAL will continue to work until 2012, and a new hard X-ray all sky survey will be carried out with the launch of HXMT. Using nearly ten years of IBIS data and the new hard X-ray telescope aboard HXMT, the source detecting threshold could be reduced to  $\sim 0.1$  mCrab for the Galactic plane and even the higher latitude regions. Thus, in our simulations, we consider the wider interest for both scientific studies and future possible different hard X-ray survey missions; we have used an energy flux threshold of  $10^{-12}$  erg cm $^{-2}$  s $^{-1}$  ( $\sim 0.05$  mCrab for the energy band of 20–100 keV) for both the plane and higher latitude regions.
8. We estimate the hard X-ray flux of young pulsars with the correlation of X-ray luminosity versus the spin-down power (see Figs. 1, 4 or 5). We firstly derive the hard X-ray luminosity from the  $L_X - L_{sd}$  relation, and assuming that the hard X-ray emission is isotropic, then calculate the X-ray flux  $F_X = L_X/4\pi d^2$ . In this simulation, two  $L_X - L_{sd}$  correlations are taken for a comparison:  $L_X = 10^{-13.6} L_{sd}^{1.31}$ , which is only from the detected young hard X-ray pulsars, and  $L_X = 10^{-21} L_{sd}^{1.5}$ . So, two simulated pulsar samples are obtained here.

## 4.2 Simulated Results

We carried out Monte Carlo simulations of the pulsars born in the past  $\sim 10$  Myr for the whole Galaxy and the Gould Belt region. For the case of  $L_X = 10^{-13.6} L_{sd}^{1.31}$ , 189 hard X-ray pulsars are found above the flux threshold of  $10^{-12}$  erg cm $^{-2}$  s $^{-1}$ ; 4 of them are produced in the Gould Belt, and 9 pulsars (3 from the Gould Belt) are located at  $b > 5^\circ$ . For the case of  $L_X = 10^{-21} L_{sd}^{1.5}$ , 110 hard X-ray pulsars are found above the flux threshold; 2 of them are produced in the Gould Belt, and only 1 pulsar (from the Gould Belt) is located at  $b > 5^\circ$ . In Figure 7, the all sky distributions of the simulated hard X-ray pulsars are plotted for two samples:  $L_X \propto L_{sd}^{1.31}$  (left panel) and  $L_X \propto L_{sd}^{1.5}$  (right panel).

In Figure 8, we plot the distributions of the pulsar periods for two pulsar samples:  $L_X \propto L_{sd}^{1.31}$  (left panel) and  $L_X \propto L_{sd}^{1.5}$  (right panel). Both sources produced in the Galaxy (blank histogram) and in the Gould Belt (hatched histogram) are also noted in all the following figures. All simulated pulsars in the samples have spin periods below 0.6 s, suggesting relatively young pulsars as potential hard X-ray sources (also see below). The hard X-ray pulsars produced in the Gould Belt have longer spin periods than those in the Galaxy. The pulsar sample from  $L_X \propto L_{sd}^{1.5}$  is younger (longer spin period) than that from  $L_X \propto L_{sd}^{1.31}$ . In the case of  $L_X \propto L_{sd}^{1.5}$ , the oldest one is the one produced in the Gould Belt, with  $P \sim 0.2$  s.

We also plot the distributions of the surface magnetic fields for two pulsar samples in Figure 9. Most hard X-ray pulsars have a magnetic field from  $10^{12} - 4 \times 10^{12}$  G, but a few of them could be

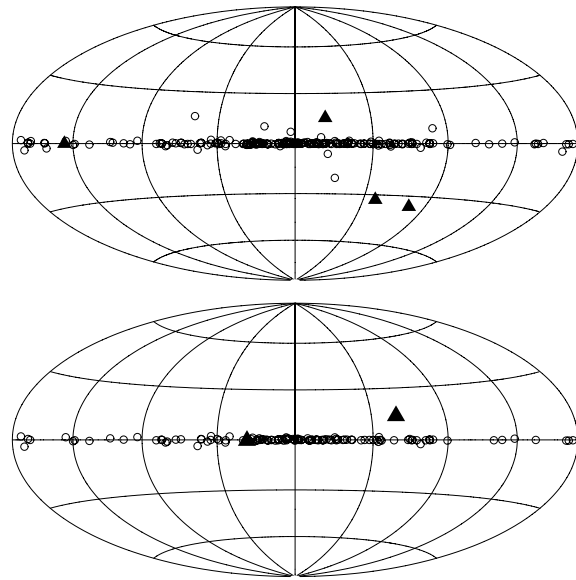


**Fig. 7** All sky distributions of the simulated hard X-ray pulsars in Galactic coordinates for two cases:  $L_X \propto L_{sd}^{1.31}$  (top) and  $\propto L_{sd}^{1.5}$  (bottom). The distributions of the pulsars produced in the Gould Belt (solid triangles), and in the Galaxy (blank circles) are also shown.

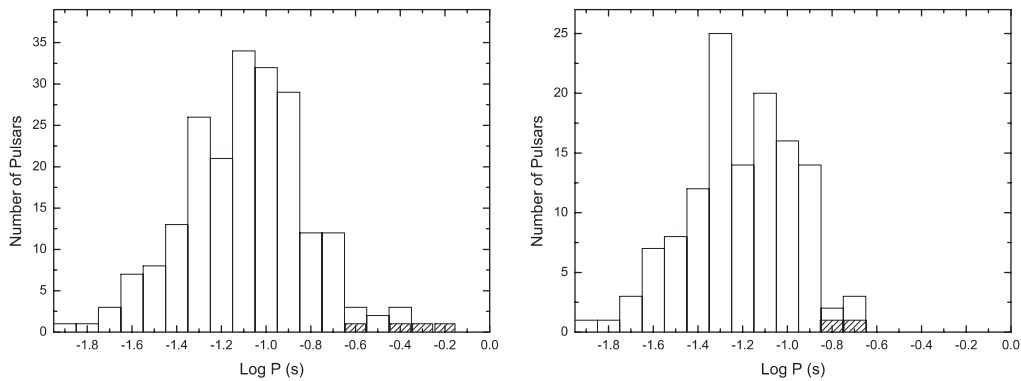


**Fig. 8** Distributions of the spin periods of the simulated hard X-ray pulsars in two cases:  $L_X \propto L_{sd}^{1.31}$  (left) and  $\propto L_{sd}^{1.5}$  (right). The distributions of the pulsars produced in the Gould Belt (hatched), and in the Galaxy (blank) are also shown.

high-magnetic-field pulsars ( $> 10^{13}$  G). In Figure 10, we show the distance distributions of simulated hard X-ray pulsars. For both simulated cases, the pulsar samples produced in the Gould Belt and the Galaxy have different distance distributions. The X-ray pulsars produced in the Gould Belt generally have a distance below  $\sim 1$  kpc, but the hard X-ray pulsar in the Galactic plane can be detected at a distance of  $> 20$  kpc. Since hard X-ray emission is nearly transparent in the ISM of the Galactic plane, future hard X-ray surveys are expected to discover more distant pulsars.

In Figure 11, the age distributions of simulated pulsars are also shown. The ages of hard X-ray pulsar candidates in the Galaxy range from  $10^3 - 10^6$  yr, while the pulsars produced in the Gould Belt

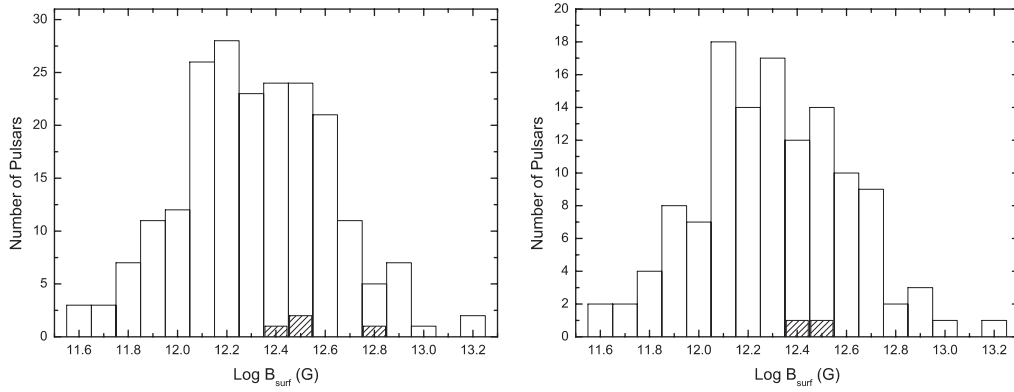


**Fig. 9** Distributions of the surface magnetic fields of the simulated hard X-ray pulsars in two cases:  $L_X \propto L_{sd}^{1.31}$  (left) and  $\propto L_{sd}^{1.5}$  (right). The distributions of the pulsars produced in the Gould Belt (hatched), and in the Galaxy (blank) are also shown.

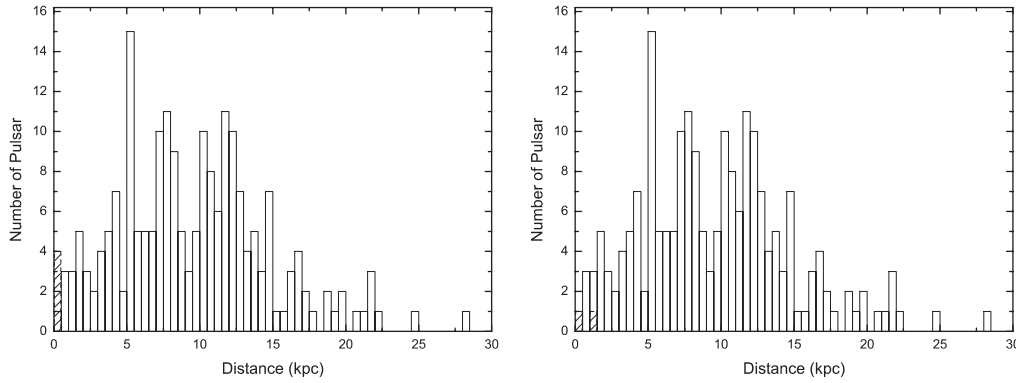


**Fig. 10** Distributions of the distances of the simulated hard X-ray pulsars in two cases:  $L_X \propto L_{sd}^{1.31}$  (left) and  $\propto L_{sd}^{1.5}$  (right). The distributions of the pulsars produced in the Gould Belt (hatched), and in the Galaxy (blank) are also shown.

have an age of  $\geq 10^5$  yr, generally older than those in the Galaxy. Figure 12 displays the hard X-ray luminosity (20–100 keV) versus the age ( $\tau$ ) of simulated hard X-ray pulsars for two samples. All hard X-ray pulsar candidates have an age of  $< 6 \times 10^5$  yr, and a 20–100 keV luminosity of  $> 3 \times 10^{30}$  erg s $^{-1}$ . For the sample from  $L_X \propto L_{sd}^{1.31}$  (left panel), the luminosity versus the age follows a correlation of  $L_X = 10^{42.9 \pm 0.4} \tau^{-1.96 \pm 0.8}$  ( $r = -0.8594$ ,  $p = < 0.0001$ ). For the case of  $L_X \propto L_{sd}^{1.5}$  (right panel), the correlation is derived as  $L_X = 10^{42.5 \pm 0.4} \tau^{-1.90 \pm 0.08}$  ( $r = -0.8249$ ,  $p = < 0.0001$ ). From both simulated pulsar samples, the derived  $L_X - \tau$  correlation is still very consistent with the relation from the observed hard X-ray pulsar sample by INTEGRAL/IBIS ( $L_X \propto \tau^{-1.8}$ , see Fig. 2).

Finally, the 20–100 keV hard X-ray flux distributions of simulated pulsars for the two samples are presented in Figure 13. The fluxes of the hard X-ray pulsars produced in the Gould Belt are below  $10^{-11}$  erg cm $^{-2}$  s $^{-1}$  (0.5 mCrab for an energy band of 20–100 keV). Therefore, these nearby hard X-ray pulsars are relatively difficult to detect with present hard X-ray surveys. We also check the hard X-ray fluxes of pulsars located in higher latitude regions ( $b > 5^\circ$ ) which are also all below 0.5 mCrab.

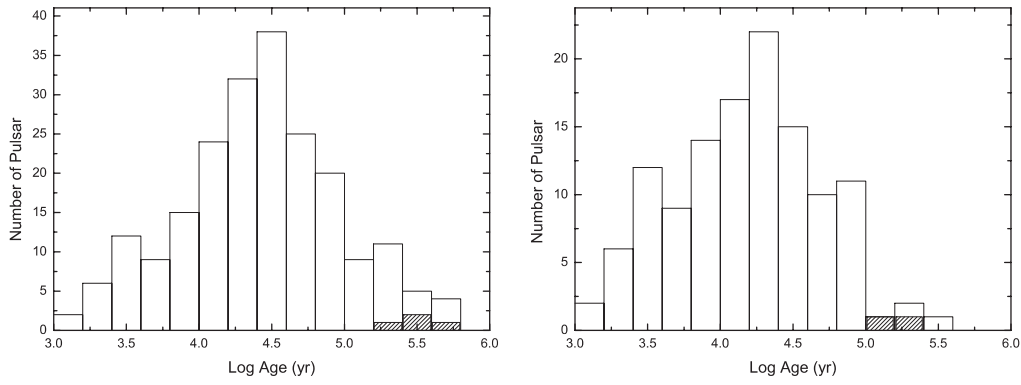


**Fig. 11** Distributions of the ages of the simulated hard X-ray pulsars in two cases:  $L_X \propto L_{sd}^{1.31}$  (left) and  $\propto L_{sd}^{1.5}$  (right). The distributions of the pulsars produced in the Gould belt (hatched), and in the Galaxy (blank) are also shown.

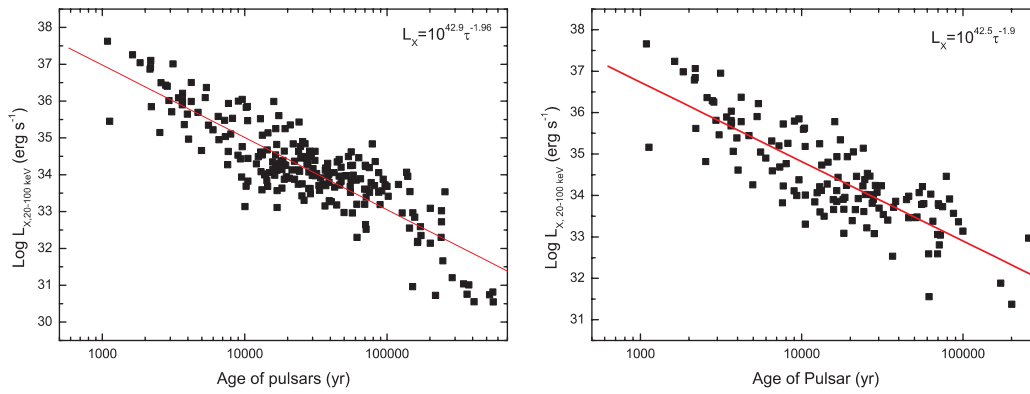


**Fig. 12** Hard X-ray luminosity (20–100 keV) versus age ( $\tau$ ) of simulated hard X-ray pulsars for two cases:  $L_X \propto L_{sd}^{1.31}$  (left) and  $\propto L_{sd}^{1.5}$  (right). The solid lines are best fitting lines:  $L_X = 10^{42.9} \tau^{-1.96}$  (left case) and  $L_X = 10^{42.5} \tau^{-1.9}$  (right case).

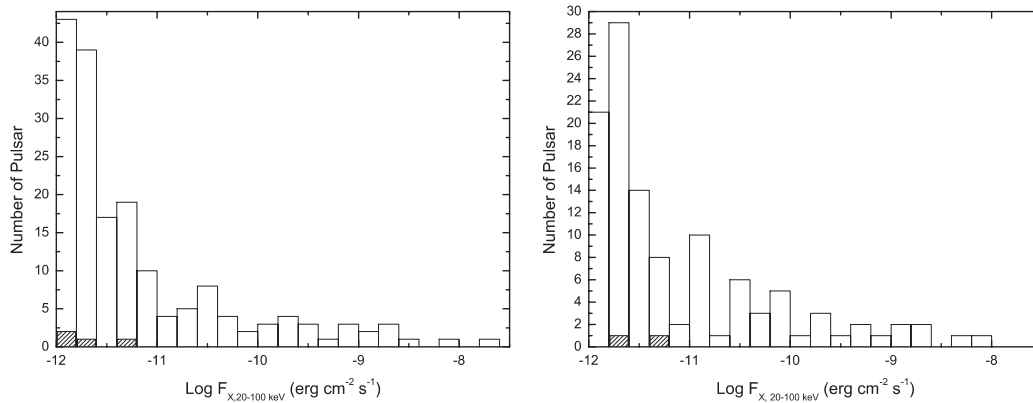


**Fig. 13** Distributions of hard X-ray flux (20–100 keV) of the simulated hard X-ray pulsars in two cases:  $L_X \propto L_{sd}^{1.31}$  (left) and  $\propto L_{sd}^{1.5}$  (right). The distributions of the pulsars produced in the Gould Belt (hatched), and in the Galaxy (blank) are also shown.

Present INTEGRAL/IBIS surveys have a sensitivity of  $\sim 0.5$  mCrab for the higher latitude region (Bird et al. 2007), so these high latitude pulsars in the Galaxy cannot yet be detected yet. The hard X-ray pulsars in the Galactic plane can be strong hard X-ray sources. For the pulsar sample from  $L_X \propto L_{sd}^{1.31}$ , nearly 1/5 of the pulsars have fluxes above  $10^{-11}$  erg cm $^{-2}$  s $^{-1}$ , and for the case of  $L_X \propto L_{sd}^{1.5}$ ,  $\sim 25\%$  of the pulsars have fluxes above  $10^{-11}$  erg cm $^{-2}$  s $^{-1}$ . These hard X-ray pulsars could contribute to the hard X-ray source population in the Galaxy, and are potential candidates for more than 100 unidentified hard X-ray sources in the third IBIS/ISGRI soft gamma-ray catalog (Bird et al. 2007).

## 5 PULSAR DETECTABILITY WITH INTEGRAL AND HXMT SURVEYS

### 5.1 INTEGRAL/IBIS

The INTEGRAL observatory will continue to work until 2012. The next 5 years of observations will concentrate on missed sky regions in past surveys. At present, the most deep survey region is the inner Galaxy where the sensitivity of INTEGRAL/IBIS has reached  $\sim 4 \times 10^{-12}$  erg cm $^{-2}$  s $^{-1}$  ( $5\sigma$ ) in the energy range of 20–100 keV. In the future, INTEGRAL observations will provide homogeneous exposure along the Galactic plane and deeper surveys of high latitude regions (mainly for extra-galactic sources).

If the survey depth of INTEGRAL/IBIS reaches  $3 \times 10^{-12}$  erg cm $^{-2}$  s $^{-1}$  (0.15 mCrab for 20–100 keV,  $5\sigma$ ) after ten years of INTEGRAL observations for the sky (at least for the Galactic plane), we expect that INTEGRAL/IBIS could discover/identify about 71 hard X-ray pulsars (one produced in the Gould Belt) from the simulated sample of  $L_X \propto L_{sd}^{1.31}$  and 45 hard X-ray pulsars in the Galaxy and one pulsar in the Gould Belt from the sample of  $L_X \propto L_{sd}^{1.5}$ .

### 5.2 HXMT

The Hard X-ray Modulation Telescope (HXMT) is a collimated hard X-ray telescope and will have the highest sensitivity and spatial power in the world after its launch. The main hard X-ray imager (20–200 keV) of HXMT is based on the direct demodulation imaging method (Li & Wu 1993) and well established NaI(Tl)/CsI(Na) phoswich detection techniques. In addition, large area silicon detectors will provide additional sensitivity in the energy band of 3–30 keV, extending the scientific capability of HXMT.

HXMT has a field view of  $5.7^\circ \times 5.7^\circ$ , and a total collecting area of about 5000 cm $^2$ . The spatial resolution is  $\sim 5'$  and the source location accuracy is less than  $1'$  in the energy range of 20–200 keV. HXMT is planned to be launched in 2011 and has a lifetime of  $\sim 3$  yr (which could be extended). It will perform an all sky hard X-ray survey, and is expected to discover more than 1000 new hard X-ray sources. The main scientific targets are active galactic nuclei (AGNs), X-ray binaries (black holes and neutron stars), pulsars and gamma-ray bursts (GRBs). So, the HXMT observations would have deep surveys of both the Galactic plane and high latitudes. After three years of HXMT observations, the survey depth of the whole sky would reach  $\sim 2 \times 10^{-12}$  erg cm $^{-2}$  s $^{-1}$  (0.1 mCrab for the energy range of 20–100 keV,  $5\sigma$ ). With its better angular resolution, HXMT is expected to resolve and identify more hard X-ray sources.

From our simulations, hard X-ray young pulsars would significantly contribute to hard X-ray populations discovered by HXMT. Above the flux threshold of  $2 \times 10^{-12}$  erg cm $^{-2}$  s $^{-1}$ , about 95 pulsars (including one pulsar produced in the Gould Belt) in the sample of  $L_X \propto L_{sd}^{1.31}$  and 61 pulsars (one in the Gould Belt) in the sample of  $L_X \propto L_{sd}^{1.5}$  could be detected.

## 6 SUMMARY AND DISCUSSION

We have presented the hard X-ray properties of rotation powered pulsars from 20–100 keV with the data of INTEGRAL/IBIS. The 10 detected pulsars have luminosities of  $10^{33} - 10^{37}$  erg s $^{-1}$  and photon indices of 1.6–2.1 in the energy range of 20–100 keV. Correlations of hard X-ray luminosity versus spin-down power and age of pulsars are found:  $L_X = 10^{-13.6 \pm 0.6} L_{sd}^{1.31 \pm 0.03}$  and

$L_X = 10^{42.2 \pm 0.8} \tau^{-1.80 \pm 0.16}$ . The derived  $L_X - L_{\text{sd}}$  relation of hard X-ray pulsars suggests that the hard X-ray emission from 20–100 keV in rotation-powered pulsars is dominated by PWN contributions.

Assuming similar spectral properties in both the 2–10 keV and 20–100 keV energy bands for pulsar and PWN components, we have predicted hard X-ray luminosities and fluxes of 39 young X-ray pulsars and 8 MSPs. We found a better correlation of X-ray luminosity and spin-down power from the predicted pulsar sample:  $L_X \propto L_{\text{sd}}^{1.5}$ . In addition, with predicted hard X-ray fluxes, about 20 known young X-ray pulsars and 1 MSP may be detected after ten years of INTEGRAL observations.

To probe the pulsar contributions to the hard X-ray sky, we have carried out Monte Carlo simulations to model the young pulsar population in the Galaxy and Gould Belt. Their 20–100 keV hard X-ray luminosities and fluxes are estimated from the  $L_X - L_{\text{sd}}$  relations:  $L_X \propto L_{\text{sd}}^{1.31}$  and  $L_X \propto L_{\text{sd}}^{1.5}$ . Two hard X-ray pulsar samples are obtained in simulations. These young hard X-ray pulsars could be detected with future INTEGRAL and HXMT surveys. According to the expected sensitivity of the two instruments, we estimate that  $> 70$  young pulsars in the  $L_X \propto L_{\text{sd}}^{1.31}$  case and  $> 40$  young pulsars in the  $L_X \propto L_{\text{sd}}^{1.5}$  case could be detected after ten years of INTEGRAL observations and the launch of HXMT. Most hard X-ray pulsars are located in the Galactic plane, so the young pulsars would be a significant population of hard X-ray sources in the sky, and will contribute to unidentified hard X-ray sources in the Galaxy with present and future hard X-ray surveys by INTEGRAL and HXMT. We should also note that the results will be affected by the uncertainties of pulsar birth rate ( $\sim 1$  per 50–150 yr) in the Galaxy and the predicted X-ray luminosity (though two correlations are used for a comparison in this work).

Millisecond pulsars are not in the simulated samples, but they would be possible hard X-ray sources. The hard X-ray emission from MSPs is attributed to relativistic pulsar winds which interact with the interstellar medium and/or a binary companion (Cheng et al. 2006). In Section 3, we have predicted the hard X-ray luminosity and flux of 8 MSPs in the Galactic field which have been detected in soft X-rays, and one MSP (PSR J0218+4232) could be detected by INTEGRAL/IBIS hard X-ray surveys. More than 2/3 of the known MSPs are located in globular clusters (see Wang 2006), so is it possible that future instruments could detect hard X-ray signals from MSPs in globular clusters? Previously, X-ray studies on MSPs in globular clusters suggested that MSPs have thermal components with  $kT \sim 0.2 - 0.3$  keV (e.g. 47 Tuc, Grindlay et al. 2002). However, recent work (Bogdanov et al. 2006) found that these MSPs in 47 Tuc exhibit a significant non-thermal component above 3 keV. This non-thermal hard X-ray emission can be produced in an intrabinary shock formed by the interaction between the relativistic wind and matter from the stellar companion (Cheng et al. 2006). It is difficult to resolve each MSP in hard X-ray surveys, but we may detect hard X-ray signals by total contribution of these MSPs in globular clusters. For 47 Tuc at a distance  $\sim 4.9$  kpc, there have been over 20 MSPs discovered up to the present, with a mean spin-down power of  $L_{\text{sd}} \sim 2 \times 10^{34}$  erg s $^{-1}$  (Cheng & Taam 2003). Assuming 20 hard X-ray MSPs located in 47 Tuc and a relation of  $L_X = 10^{-21} L_{\text{sd}}^{1.5}$  applied, we predict a hard X-ray flux of  $\sim 10^{-13}$  erg cm $^{-2}$  s $^{-1}$  in the energy range of 20–100 keV, well below the sensitivity of INTEGRAL and HXMT. Anyway, detection of hard X-ray emission from globular clusters above 3 keV may help us to estimate the number of unresolved MSPs in globular clusters.

Studying the hard X-ray properties of rotation-powered pulsars can help to understand the shock wave physics in pulsar wind nebulae and resolve different acceleration models inside the pulsar magnetosphere. From observations of soft X-ray bands, the spectra of the PWN component can be extended to 10 keV without significant spectral cut-off, so the synchrotron radiation of relativistic electrons accelerated in shock waves of PWNe should show spectral cut-off in hard X-ray bands (also see Forot et al. 2006; McBride et al. 2008). The synchrotron spectral index and cut-off will constrain some poorly-defined parameters of PWNe, like pulsar wind particle energy and magnetic field. Pulsed hard X-ray emission properties have not been well studied with present popular gap models. This nonthermal emission (above 2 keV) may be produced in the vicinity of the polar cap as a result of inverse Compton scattering of higher order generation pairs of particles on soft photons emitted by the neutron star (Zhang & Harding 2000) or in the outer magnetosphere as a result of synchrotron radiation of downward cascades from the outer gap electron/positron particles (Cheng & Zhang 1999). Therefore, hard X-ray emission from 10 keV to hundreds of keV may have multiple contributions or different radiation mechanisms. One of the best ways to resolve different gap models or different radiation mechanisms will be a phase-

resolved spectral analysis of hard X-ray pulsars. The analysis now can be carried out on the brightest one, the Crab pulsar, and in the future on weaker X-ray pulsars with more observations and new instruments.

**Acknowledgements** We are grateful to the referee for comments improving the manuscript and also to Profs. K. S. Cheng and J. L. Han for the fruitful discussions. This work is supported by the National Natural Science Foundation of China (Grant Nos. 10803009 and 10833003).

## References

- Abdo, A. A., et al. 2008, *Science*, 322, 1218  
Abdo, A. A., et al. 2009, *ApJS*, 183, 46  
Bhattacharya, D., Wijers, R. A. M. J., Hartman, J. W., & Verbunt, F. 1992, *A&A*, 254, 198  
Becker, W., & Trümper, J. 1997, *A&A*, 326, 682  
Becker, W., & Aschenbach, B. 2002, *Neutron Stars, Pulsars and Supernova Remnants*, eds. W. Becker, H. Lesch, & J. Trümper, MPE Report 278, 64 (BA02)  
Bird, A. J., et al. 2007, *ApJS*, 170, 175  
Bogdanov, S., et al. 2006, *ApJ*, 646, 1104  
Camilo, F., et al. 2004, *ApJ*, 616, 1118 (CG04)  
Campana, R., et al. 2008, *MNRAS*, 389, 691  
Caraveo, P. A., et al. 2003, *Science*, 301, 1345 (CA03)  
Chen, Y., et al. 2006, *ApJ*, 651, 237 (CH06)  
Cheng, K. S., & Taam, R. E. 2003, *ApJ*, 598, 1207  
Cheng, K. S., Taam, R. E., & Wang, W. 2004, *ApJ*, 617, 480  
Cheng, K. S., Taam, R. E., & Wang, W. 2006, *ApJ*, 641, 427  
Cheng, K. S., & Zhang, L. 1999, *ApJ*, 515, 337  
Dean, A. J., et al. 2008a, *MNRAS*, 384, L29  
Dean, A. J., et al. 2008b, *Science*, 321, 1183  
De Luca, A., et al. 2005, *ApJ*, 623, 1051 (DE05)  
De Rosa, A., et al. 2009, *MNRAS*, 393, 527  
Forot, M., et al. 2006, *ApJ*, 651, L45  
Gaensler, B. M., et al. 2002, *ApJ*, 569, 878 (GA02)  
Gaensler, B. M., et al. 2003, *ApJ*, 588, 441 (GA03)  
Gaensler, B. M., et al. 2004, *ApJ*, 616, 383 (GA04)  
Gotthelf, E. V., & Halpern, J. P. 2008, *ApJ*, 681, 515 (GH08)  
Gonzalez, M. E., & Safi-Harb, S. 2003, *ApJ*, 591, L143 (GN03)  
Gonzalez, M. E., et al. 2006, *ApJ*, 652, 569 (GN06)  
Grenier, I. A. 2000, *A&A*, 364, L93  
Grindlay, J. E., et al. 2002, *ApJ*, 581, 470  
Guillout, P., et al. 1998, *A&A*, 337, 113  
Halpern, J. P., et al. 2001, *ApJ*, 552, L125 (HL01)  
Helfand, D. J., Gotthelf, E. V., & Halpern, J. P. 2001, *ApJ*, 556, 380 (HE01)  
Helfand, D. J., Collins, B. F., & Halpern, J. P. 2003, *ApJ*, 582, 783 (HF03)  
Hessels, J. W. T., et al. 2004, *ApJ*, 612, 389 (HS04)  
Hinton, J. A., et al. 2007, *A&A*, 476, L25 (HI07)  
Hughes, J. P., et al. 2001, *ApJ*, 559, L153 (HU01)  
Kaaret, P., et al. 2003, *ApJ*, 546, 1159 (KA03)  
Kargaltsev, O., & Pavlov, G. G. 2007, *ApJ*, 670, 655 (KP07a)  
Kargaltsev, O., Pavlov, G. G., & Garmire, G. P. 2007, *ApJ*, 660, 1413 (KP07b)  
Kargaltsev, O., & Pavlov, G. G. 2008, in *AIP Conf. Ser. 983, 40 Years of Pulsars: Millisecond Pulsars, Magnetars and More* (Melville, NY: AIP), 171 (arxiv:0801.2602)  
Kaspi, V. M., et al. 2001, *ApJ*, 562, L163 (KI01)  
Kramer, M., et al. 2003, *MNRAS*, 342, 1299 (KR03)

- Kuiper, L., et al. 2000, *A&A*, 359, 615
- Kuiper, L., Hermsen, W., & Stappers, B. 2004, *Advances in Space Research*, 33, 507
- Li, T. P., & Wu, M. 1993, *Ap&SS*, 206, 91
- Li, X. H., Lu, F. J., & Li, T. P. 2005, *ApJ*, 628, 931 (LI05)
- Li, X. H., Lu, F. J., & Li, Z. 2008, *ApJ*, 682, 1166
- Lorimer, D. R., Bailes, M., & Harrison, P. A. 1997, *MNRAS*, 289, 592
- Lu, F. J., et al. 2002, *ApJ*, 568, L49 (LU02)
- McBride, V. A., et al. 2008, *A&A*, 477, 249
- McGowan, K. E., et al. 2006, *ApJ*, 647, 1300 (MC06)
- Mineo, T., et al. 2006, *A&A*, 450, 617
- Mori, K., et al. 2004, *ApJ*, 609, 186 (MO04)
- Ng, C. Y., Roberts, M. S. E., & Romani, R. W. 2005, *ApJ*, 627, 904 (NG05)
- Nicastro, L., et al. 2004, *A&A*, 413, 1065 (NI04)
- Paczynski, B. 1990, *ApJ*, 348, 485
- Petre, R., Kuntz, K. D., & Shelton, R. L. 2002, *ApJ*, 579, 404 (PE02)
- Possenti, A., et al. 2002, *A&A*, 387, 993
- Roberts, M. S. E., et al. 2003, *ApJ*, 588, 992 (RB03)
- Romani, R. W., & Ng, C. Y. 2003, *ApJ*, 585, L41 (RO03)
- Romani, R. W., et al. 2005, *ApJ*, 631, 480 (RN05)
- Safi-Harb, S., et al. 2001, *ApJ*, 561, 308 (SH01)
- Saito, Y. 1998, Ph.D. Thesis, Univ. of Tokyo
- Sakurai, I., et al. 2001, *PASJ*, 53, 535 (SA01)
- Seward, F. D., & Wang, Z. R. 1988, *ApJ*, 332, 199
- Slane, P., et al. 2004, *ApJ*, 616, 403 (SL04)
- Stappers, B. W., Gaensler, B. M., Kaspi, V. M., van der Klis, M., & Lewin, W. H. G. 2003, *Science*, 299, 1372 (ST03)
- Sturmer, S. J., & Dermer, C. D. 1996, *ApJ*, 461, 872
- Thompson, D. J. 2001, in *AIP Conf. Ser. 558, High Energy Gamma-Ray Astronomy*, eds. F. A. Aharonian, & H. J. Völk (New York: AIP), 103
- Torii, K., et al. 2001, *ApJ*, 551, L151 (TO01)
- Wang, W., & Zhao, Y. 2004, *ApJ*, 601, 1038
- Wang, W., et al. 2005, *MNRAS*, 360, 646
- Wang, W. 2006, *ChJAA (Chin. J. Astron. Astrophys.)*, 6S2, 268
- Webb, N. A., Olive, J.-F., & Barret, D. 2004a, *A&A*, 417, 181 (WE04a)
- Webb, N. A., et al. 2004, *A&A*, 419, 269 (WE04b)
- Winkler, C., et al. 2003, *A&A*, 411, L1
- Zavlin, V. E., et al. 2002, *ApJ*, 569, 894 (ZA02)
- Zavlin, V. E., et al. 2007, *ApJ*, 665, L143 (ZA07)
- Zhang, B., & Harding, A. K. 2000, *ApJ*, 532, 1150